PORE NETWORK MODELING OF EXPERIMENTAL CAPILLARY PRESSURE HYSTERESIS RELATIONSHIPS

Behrooz Raeesi*, Norman Morrow, Geoffrey Mason
University of Wyoming

This paper was prepared for presentation at the International Symposium of the Society of Core Analysts held in Napa Valley, California,, USA, 16-19 September, 2013.

ABSTRACT

Increasingly sophisticated pore network models are being developed for prediction of multi-phase transport properties. The most direct method for testing a deterministic pore network model is in the prediction of capillary pressure relationships. Matching and ultimately prediction of the experimental capillary pressure hysteresis data provides a stringent test of network modeling and key guidance in further development. High quality capillary pressure hysteresis data for Bentheim sandstone are presented that include multiple scanning curves with more detail than any previously reported for consolidated sandstones. The initial model gave far less hysteresis and more NWP trapping than shown by experimental data. The numerical pore network was tuned to the capillary pressure data. Residual trapped Non-Wetting Phase, NWP, saturations given by the model were always too high. A good fit was achieved by the physically justifiable approach of not allowing snap-off in throats that had a length/diameter ratio of less than π. The highly tuned model gave a satisfactory match with scanning curves measured within the main hysteresis loop. Analysis of the distribution of trapped clusters of NWP at the end point of the modeled imbibition shows close agreement with image based measurements reported by Prodanović, et al. [1].

INTRODUCTION

Computational pore network models have been used to investigate the effects of pore space structure and pore-scale displacements on macroscopic properties such as capillary pressure and capillary hysteresis and associated phenomena such as fluid trapping in porous media and relative permeability. The simplified pore space is usually a 2D or 3D network of interconnected capillary tubes of various radii defined by a size distribution function using an approach pioneered by Fatt [2]. In most early networks, the pore throats were modeled as uniform cylinders of circular cross section in a regular lattice [2-5]. Circular cross section limits the fluid occupancy in a tube to only one phase at a time and, after displacement, hydraulic connectivity of the wetting phase can be lost. Natural porous media usually maintain some degree of hydraulic connectivity through retention of bulk water in corners and irregularities (roughness) on the solid surface. Mason and Morrow [6] proposed use of angular tubes which can hold the wetting phase in the corners and non-wetting phase in their bulk volume (dual occupancy) as a more realistic model for displacement in rocks. Analytical solutions were given for drainage and imbibition displacement capillary pressures for all shapes of triangles in terms of a shape factor. Bakke and Øren [7] were first to model sandstone as a network that incorporated

triangular pores and throats. The approach of employing pores with corners to give dual phase occupancy in individual tubes has since been widely applied in network modeling of porous media [8-13].

An important factor in the design of a more realistic network is deriving geometrical and topological parameters that are representative of real porous media. These parameters include relative location of pores, pore and throat size distributions, shape factors, coordination numbers (i.e., number of throats for each pore), size correlations between neighboring pores and between each pore and its throats, etc. Examples are deriving geometrical data from a random packing of spheres [14-16], numerical reconstruction of the geologic processes of formation of sandstones [7,8] or more recently, from high resolution X-ray micro-tomography data [10,17-19]. In addition to the complexity and cost of such methods, translating the complex features of the pore space within a rock to the simplified geometries of a network of capillary tubes is always subject to interpretation. Predicting experimental drainage capillary pressure curves purely from analysis of pore space images, at least for very strongly wetted conditions, provides a significant first step in testing the interpretation of imaging data and assessment of the predictive capability of derived network models. A more stringent test of the network model is to predict both drainage and imbibition curves, and intermediate capillary hysteresis loops. However, in most cases, only a primary drainage match has been reported [7,12]. Capillary pressure hysteresis data on their own contain important information about different aspects of pore systems and can be used to tune properties of a pore network. Valvatne and Blunt [13] tuned the parameters of the pore network that Lerdahl et al. (LOB) [10] developed for a sandstone by a process based approach, and obtained a reasonable match with the experimental air-water hysteresis data for an unconsolidated soil. Their tuned network however over-predicted the amount of trapped NWP saturation at the end of imbibition. In the present work, the code developed by Valvatne and Blunt [13] for modeling pseudo-quasi-static two-phase displacement in pore networks is adapted, together with the LOB pore network [10], to compare the modeled capillary pressure curves with extensive experimental capillary pressure hysteresis data that were recently obtained for a consolidated sandstone. The pore network parameters were then tuned, while keeping the main skeleton of the network unchanged, to establish a match with experimental primary drainage and main imbibition curves. It is shown that by applying a physically justifiable snap-off rule, the NWP residual saturation can also be matched. The tuned network successfully predicts the intermediate hysteresis loops and residual NWP saturations and provides significant insight into the modeling of capillary displacement and trapping mechanisms.

PORE NETWORK MODEL

The pore network is defined by a set of geometrical data including the number of pores and throats, and arrays including the values of shape factor, inscribed radius, volume, and spatial co-ordinates for each pore and throat. The LOB pore network is composed of 38,495 interconnected capillary tubes (12349 pore bodies and 26146 pore throats) of mostly triangular cross-section (G=0.0022-0.0481) in a 3×3×3 mm space giving an

effective porosity of 18.3%. The average coordination number (number of throats per pore) is 4.2 and the average pore-to-throat aspect ratio, α, is 2.99.

The displacement model uses a pseudo-quasi-static approach in which displacements are ranked according to capillary pressure. After each step change in the external capillary pressure, displacement occurs in the capillaries (pore or throat) that are, or become, accessed by the invading phase. For simulating primary drainage, the network model is initially saturated with wetting phase, say water. The inlet face of the network is in contact with the NWP. The contact angle is zero, i.e. water will spread against the NWP over the solid surfaces. Capillary pressure is raised in steps. At the entry capillary pressure, a main terminal meniscus (MTM) displaces water from the center of the pore throats at the inlet face. The displacement mechanism is piston-like. Piston-like displacement of the bulk water in angular tubes leaves water in the corners and the as the capillary pressure is increased in the next pressure steps, gradual recession of Arc Menisci (AMs) into the corners further reduces water saturation in the drained tubes.

During imbibition, the capillary pressure is lowered and the same displacement mechanisms take place in the opposite direction (piston-like imbibition and water encroachment in the corners). However, when AMs in corners overlap, the wetting phase spontaneously redistributes to span the pore by a process known as snap-off. When the advancing contact angle is zero, this happens when the radius of the AM is equal to the inscribed radius, R_{ins}, of the triangular cross section [6]. The pressure for snap-off, P_c^{SO}, is given by Eq. 1. For any individual tube, the snap-off capillary pressure is always smaller than the pressure of piston-like displacement, P_c^{PL}, given by advance of an MTM, Eq. 2:

$$P_c^{so} = \frac{\sigma}{R_{ins}} \tag{1}$$

$$P_c^{PL} = \frac{\sigma\,(1+2G\sqrt{\frac{\pi}{G}})}{R_{ins}} \tag{2}$$

Therefore, piston-like displacement in the model is preferred to snap-off in pore throats that are accessible by an invading MTM. However, because it is assumed that WP is connected throughout the network, snap-off can take place in any pore/throat with corners when the snap-off capillary pressure for that pore/throat is met. Each snap-off displacement creates two new back-to-back MTMs that can become new sites for piston-like displacements. In practice, even within a single triangular tube of uniform cross section, there is hysteresis and trapping of the NWP [6]. In the adapted model, for simplicity, it is assumed that after snap-off the entire volume of the tube is filled with the WP. A major contribution to NWP trapping during imbibition is by disconnection of NWP in clusters of pores. This has been demonstrated in detail for micro-models and sandstones [20] and for tube network models [21]. After each snap-off or piston-like displacement, a continuity check is made to identify disconnected clusters of NWP. When all the remaining NWP is trapped, no further displacements can take place and

imbibition is terminated at the residual NWP end point. After imbibition, the process can be reversed to obtain a secondary drainage curve. As for primary drainage, the measured NWP pressure for second drainage is increased to the entry capillary pressure. When a throat adjacent to a trapped NWP cluster is drained, the cluster reconnects to the continuous NWP and its capillary pressure is set equal to that of the continuous NWP.

RESULTS

The modeled primary drainage curve for the LOB pore network was compared to the experimental air/water capillary pressure data, reported by Raeesi [22] for three different sandstones (Boise, Berea, Bentheim). It was found that the simulated curve is similar to the primary drainage curve for Bentheim as shown in Fig. 1a. Because of the fit given between the model and experimental data for drainage of Bentheim sandstone and the large range of desaturation, further development of the model was focused on matching the model with extensive air/brine hysteresis data obtained for Bentheim sandstone given in Fig. 1b. Also, for comparison, the hysteresis loops modeled for the LOB network are presented in Fig. 1c. The entry pressure for the modeled secondary drainage curves is the same as that of the primary drainage curve, which is consistent with the experimental data. However, the difference between the imbibition and secondary drainage pressures is too low compared with the experimental data shown in Fig. 1b. The ratio of the imbibition termination pressures to the drainage entry pressure, P_T/P_E for the LOB network, is 0.87. This value is 0.53 for Bentheim. P_T/P_E ratios for the three sandstones were in the range 0.46-0.53 [22]. Even for unconsolidated porous media P_T/P_E is always less than 0.71 [23]. The high P_T/P_E ratio for the LOB network causes the modeled hysteresis loops to enclose only small areas (see Fig. 1c). A physically obvious way of lowering the imbibition termination pressure is to increase the aspect ratio (ratio of the pore body radius to the throat radius) by lowering throat radii or increasing pore radii by a constant factor. Aspect ratios for the LOB network range from 1-50, averaging 2.99. However, about half of the aspect ratios in the LOB network are 1. The effect of network average aspect ratio, α, on drainage and imbibition curves was investigated by varying the throat radii by a fixed factor while keeping pore radii constant. The results are shown in Fig. 1d. As the average aspect ratio is increased, the imbibition curve shifts down, to give lowered termination pressure and increased hysteresis, but the NWP trapping is much higher than given by experiment (cf. Figs. 1b and d).

Closer analysis of the displacement details showed that as the aspect ratio increased, snap-off increases during imbibition. For perfectly wetting conditions, the displacement pressures for piston-like drainage and imbibition are equal. However, the capillary pressure for snap-off is smaller than that of piston-like displacement. Therefore, as the number of snap-off displacements increases, so does the pressure difference between drainage and imbibition. Snap-off also increases the amount of trapping by disconnecting NWP in single pores or clusters.

A sensitivity analysis was made by modifying other LOB parameters such as pore size distribution, spatial correlation among pores, and coordination number and observing

their effects on capillary pressure curves and residual NWP saturation. The relative locations of the pores were kept unchanged. A new pore size distribution function was defined with adjustable properties such as standard deviation and average radius [22]. In order to determine throat sizes, an adjustable parameter was defined as the network minimum aspect ratio. Each throat connects two pores; the radius of the smaller pore was divided by the minimum aspect ratio, α_{min} to determine the throat radius. The effect of spatial correlation between pores was also studied. Pore radii were distributed one by one in a random manner, with a constraint that for every two neighboring connected pores, $|R_{p1}-R_{p2}| < c \times MIN(R_{p1},R_{p2})$, where $c>0$ is an adjustable parameter with lower values allowing smaller differences between the neighboring pore radii.

The qualitative effects of various parameters on primary drainage and imbibition curves are summarized in Table 1.

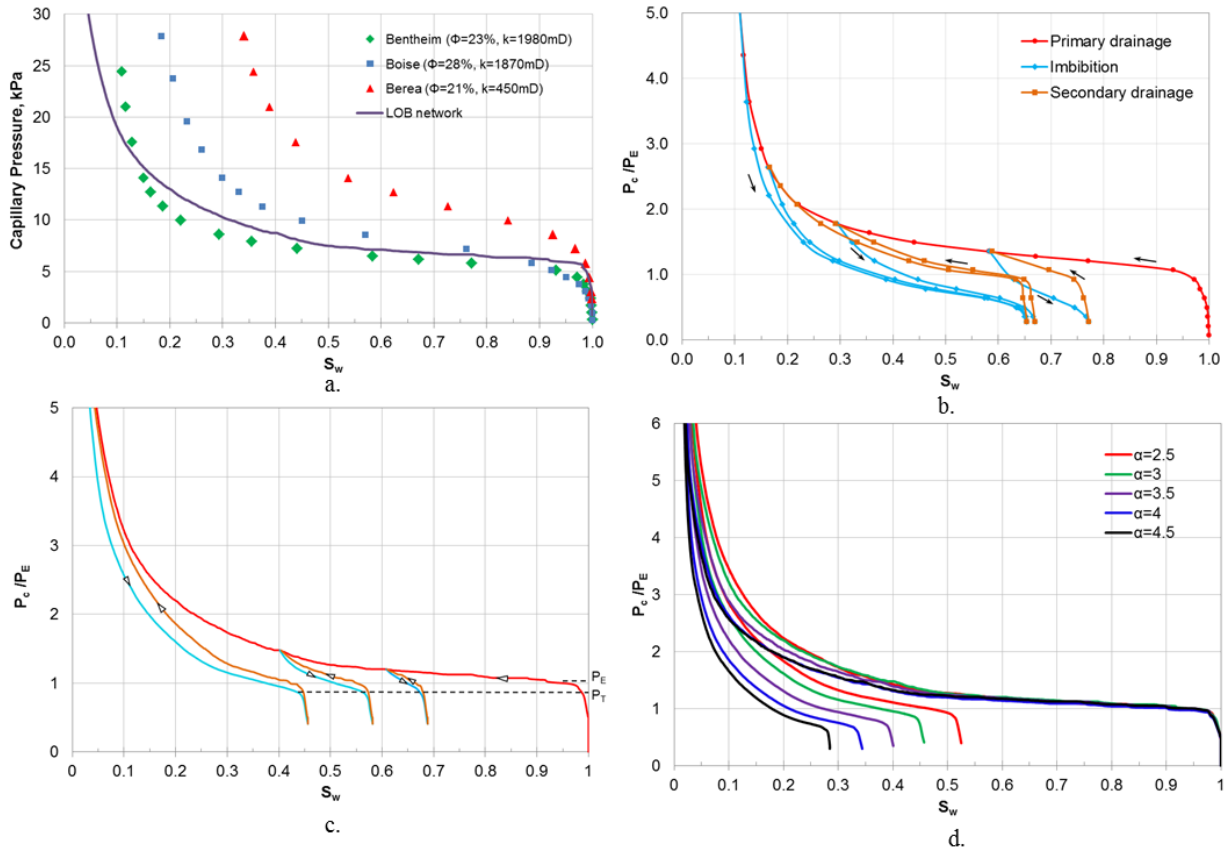

Fig. 1. Experimental and modeled capillary pressure curves. (a) Comparison of the primary drainage predicted by LOB parameters with experimental air-water data for three sandstones. (b) Measured capillary pressure hysteresis data for Bentheim sandstone. (c) Modeled capillary pressure hysteresis using the original LOB pore network parameters. (d) Modeled effect of average aspect ratio on drainage and imbibition scanning curves computed by pore network modeling. The imbibition pressures are lowered but the fractional trapping of NWP is increased.

Table 1. Summary of the effects of various pore network parameters (increase or decrease) on Primary Drainage Curves and Main Imbibition Curves (PDC and MIC respectively). α and C_n are average aspect ratio and coordination number respectively. Std. Dev. refers to the pore size distribution standard deviation.

	S_w @ P_E	Slope of PDC	Slope of MIC	P_T/P_E	S_{nwr}
Spatial corr.	-	↗	-	-	↘
Std. Dev.	↗	↗	-	-	↗
α_{min}	-	↘	↗	↘	↗
C_n	-	↘	↘	-	↘

Tuning the Pore Network to Bentheim Capillary Pressure Data

The network parameters were tuned by a manual iteration process to match primary drainage and the main hysteresis loop (imbibition-second drainage) simultaneously for Bentheim, see Fig 2a. The size of the network was scaled (i.e. coordinates of each pore was multiplied by a constant) to match the porosity and absolute permeability of the Bentheim sandstone. Fig 2a shows the best match found. In order to minimize S_{nwr}, a spatial correlation between neighboring pores was also applied. The minimum aspect ratio, α_{min}, was increased until the separation of the hysteresis loop and P_T/P_E matched that of the data. As shown in Fig. 2a, the modeled imbibition curve fits the data closely for the most part, but it is terminated at a much higher NWP residual saturation (54%) than determined by experiment (36% for gas and 43% for refined oil, [22]). Valvatne and Blunt [13] and Pentland et al. [24] also reported a similar situation where the modeled S_{nwr} were larger than the experimental data for a sand pack and different sandstones, respectively. In order to match trapping accurately, Pentland et al. [24] increased the effective imbibition contact angle in the model by assuming a uniform distribution of advancing contact angles ranging from 35° to 65°. However, increase in intrinsic contact angles over this range has been shown to give marked reduction in imbibition capillary pressures [25]. For the experiments described by Pentland et al. [24] and those of the present work, there is a strong case for assuming that the effective contact angles for drainage and imbibition are zero.

The early termination of imbibition is related to the high proportion (95%) of snap-offs in the throats that occurs when the corner AMs overlap. However, this criterion is only physically realistic when the length/diameter ratio of the tube is greater than the critical value at which the liquid bridge in the pore throat becomes unstable and ruptures. In theory, a cylindrical bridge becomes unstable when the length/diameter ratio exceeds a critical value equal to π [26-28]. Mason [27] measured this value and reported values very close to π (between 3.140 and 3.1417). This criterion was applied in the model by not allowing snap-off in throats with length/diameter ratio less than π. Throat lengths were adjusted by slight adjustment of the size of the network (stretching) to obtain the residual saturation of 35%, which is the experimental value for trapping (see Fig 2b). During this process, porosity was held constant by adjusting pore volumes using a constant factor. This could also be done by adjusting the critical length/diameter instead of throat lengths. Table 2 summarizes the properties of the modified network.

Table 2. Specifications of the equivalent pore network obtained for Bentheim sandstone

Item	Pores	Throats	Total
Network dimensions (mm)	-	-	4.02
Average shape factor	0.025	0.025	0.025
Min. inscribed radius (μm)	6.6	3.0	3.0
Max. inscribed radius (μm)	78.9	35.2	78.9
Ave. inscribed radius (μm)	34.4	13.7	20.3
Ave. coordination number	4.2	-	-
Ave. aspect ratio	-	-	2.55
Min. aspect ratio	-	-	2.20
Max. aspect ratio	-	-	10.97
Network porosity (%)	14.2	7.0	21.2
Microporosity (%)	-	-	2.0
Total Porosity (%)	-	-	23.2
Absolute permeability (mD)	-	-	2450

The number of snap-offs during the main imbibition after applying this criterion was decreased from 97% of the total displacements (81% of the throats) to 47% (45% of the throats). This reduced the NWP entrapment by allowing more pores/throats to be swept by piston-like imbibition. The sensitivity of S_{nwr} and snap-off rate to the value of critical length/diameter ratio is shown in Fig. 2c. The number of snap-offs and S_{nwr} both decrease by increasing the critical ratio. However, S_{nwr} reaches a lower limit of 0.29, which reflects the amount of NWP trapping mainly by piston-like imbibition.

The network model was then used, without any further adjustments, to predict the hysteresis cycles starting from different initial saturations. The predicted curves are in close agreement with the experimental curves (Fig. 2d). The model tends to under predict trapping for the imbibition scanning curves, but only by about 1 or 2%. The total number of throats satisfying the critical length/diameter criterion for snap-off decreases significantly for hysteresis cycles starting from higher initial water saturations (i.e. smaller capillary pressures). As S_{wi} increases, the average radii of throats invaded during drainage increases (larger throats are drained first) as does the number of throats that satisfy the critical length/diameter ratio for snap-off. Therefore, at high initial wetting phase saturations, imbibition is mainly controlled by piston-like displacements. For example, during imbibition starting from Point 1 in Fig. 2d, 86.5% of the total displacements are piston-like. This fraction decreases to 73.7% and 61.7% for imbibition curves starting at Points 2 and 3, respectively.

Distribution of Trapped NWP Given by the Network Model

The size distribution of the trapped NWP blobs at the residual NWP saturation is of particular interest. Relationships between trapped and continuous fractions of NWP, postulated by Morrow and Harris [29], were determined from the network model (see Fig. 2e). Most trapping, in terms of volume, takes place at low capillary pressures close to the imbibition termination pressure. Companion loops for trapping and reconnection, similar to that shown in Fig. 2e, can be generated from the model for all of the scanning loops. The computed numbers of snap-offs and piston-like displacements as a function of

imbibed wetting phase saturation are shown in Fig. 2f. This figure indicates that increase in S_w early in the imbibition process is mainly due to water encroachment and snap-off in the corners, while at lower capillary pressures piston-like becomes the dominant mechanism.

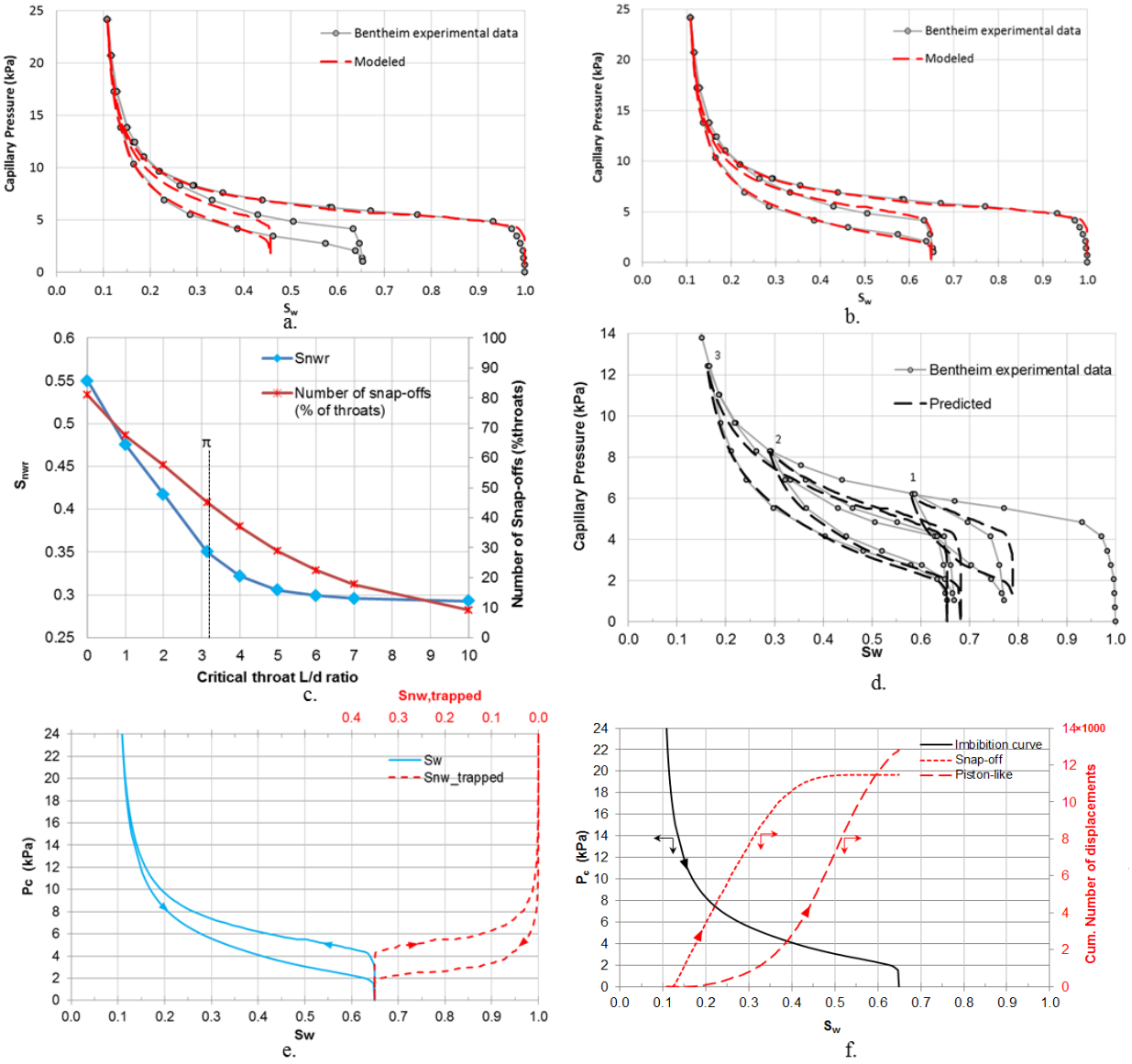

Fig. 2. Comparison of experimental and modeled capillary pressure relationships for Bentheim Sandstone: (a) Modeled capillary pressure curves, after tuning LOB parameters. (b) Modeled capillary pressure curves after applying a snap-off criteria based on pore-length. (c) Change in the NWP residual saturation and number of snap-offs with length/diameter ratio. (d) Predicted capillary pressure scanning loops starting from the fitted primary drainage and main imbibition curve. (e) Trapped NWP saturation as a function of capillary pressure during imbibition and secondary drainage derived from network modeling. (f) Cumulative number of piston-like and snap-off displacements as a function of water saturation during imbibition.

The number and volume distributions of the trapped NWP blob size at the residual saturation for the main imbibition curve (S_{wi}=0.11) are given in Fig. 3a. Singlets and doublets (1 and 2 pores per blob, respectively) compose 65.9% and 15.2% of the total number of NWP blobs, respectively. However, these blobs account for only small fractions of the total trapped NWP volume (12.7% for singlets and 8.1%, for doublets). 60.3% of the NWP residual saturation volume is trapped in clusters of 6 or more pores. Chatzis et al. [30] reported that 50% of the solidified NWP blob sizes at the residual saturation in Berea sandstone fall in the range of pore sizes measured previously from resin pore casts for a similar Berea sandstone. This agrees with the network model results. Most of the singlets are trapped by snap-off at high capillary pressures.

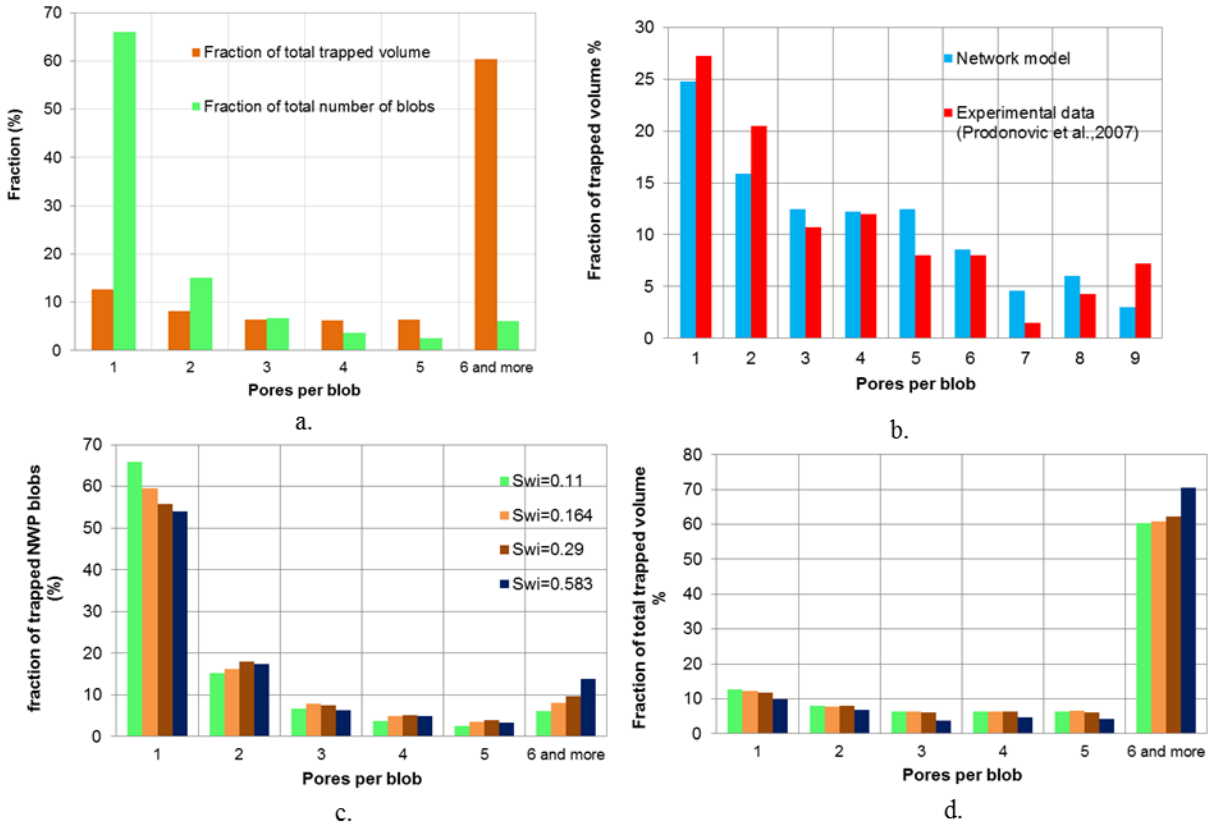

Figure 3. Details of blob sizes by number and volume. (a) Modeled distribution of trapped NWP blobs. (b) Comparison of modeled distribution of NWP blobs occupying 9 pores or less for Bentheim sandstone with experimental data for Berea sandstone. (c) Modeled number distribution of residual NWP blobs starting at different initial water saturations (corresponding to the imbibition curves shown in Figs. 1b). (d) Modeled volume distribution of blobs by size.

The modeled blob distributions are compared in Fig 3b with those obtained by synchrotron imaging of a brine/hexadecane/Berea sandstone system at S_{nwr} [1]. A search algorithm was based on variations in cross-sectional area. The singlet frequency was 60% and the doublet frequency was 25%. They noted that the number did not include blobs smaller than 1.2×10^{-5} mm^3. To eliminate the error caused by the lower cut-off on blob

sizes, Prodanović et al. [1] also reported the volume fraction of the blobs by considering only the blobs that occupy from 1 to 9 pores. Blobs occupying clusters greater than 9 pores were excluded. Blob distributions obtained by the network model were compared with the experimental data of Prodonović et al. [1]. The volume of each trapped NWP cluster at residual oil saturation was divided by the sum of the volumes of all trapped clusters occupying 9 pores or less to obtain the fraction of trapped volume. The comparison is presented in Fig. 3b. Agreement between the distribution derived from the model and the experimental data of Prodonović et al. [1] is excellent for most blob sizes.

It is also of interest to investigate the effect of initial WP saturation (S_{wi}) on the NWP blob distribution at S_{nwr}. Fig. 3c shows the number and volume fraction for NWP blobs at residual saturation for 4 modeled imbibition curves starting at initial water saturations of 11.0%, 16.4%, 29.0%, and 58.3%. As seen in this figure, number fraction and volume fraction for singlets slightly decreases with S_{wi}, whereas the number and volume fraction of blobs occupying 6 or more pores increases with S_{wi}. This is again consistent with previous discussion of the effect of snap-off versus piston-like displacement on blob sizes. Kumar et al. [31] used micro CT imaging to study the effect of S_{wi} on the residual NWP blob size distribution in Fontainbleau sandstone samples. Their results showed that the median blob size increased with S_{wi}. It is also evident from their reported cumulative blob size distributions that the number of singlets decreases with increase in Swi. This supports the validity of the predicted residual blob distributions given by starting at different initial wetting phase saturations.

Concluding Remarks

Comprehensive data on capillary pressure hysteresis for rocks has been matched by tuning a network model. Numerous parameters are involved, so the solutions are obviously not unique. In spite of the numerous adjustable parameters, matching the imbibition data still required additional adjustment of the displacement mechanism that is in common use. Experimental data shows consistently less trapping for air versus oil as the non-wetting phase [22]. Further fine tuning of the model, likely related to identifying the mechanism of viscosity and viscosity ratio effects on trapping, is anticipated.

While most network models have been aimed at determining transport properties such as relative permeability, this application does not reflect the power of network modeling to provide detailed account of the displacement mechanism. For example, the ability to track percolation effects and to identify the fraction of trapped versus continuous oil phase. The next and more stringent challenge of network modeling is to use micro CT images of the rock pore space to develop detailed capillary hysteresis data and relative permeability. For realistic modeling, at some stage, issues such as the significant effects of colloidal dispersion and swelling on flow need to be addressed. They can reduce the ratio of brine to air permeabilities of a rock by about one half and often far more. These reductions cannot simply be scaled to account for their effect on relative permeability. For water-wet colloids, much greater effects on water versus oil relative permeabilities will need to be taken into account. Nevertheless, predictive modeling of two phase

behavior under very strongly wetted conditions will provide a sound platform for investigation of the far more complicated effects of wettability given by changes induced by adsorption from crude oil. Observed dependency of wettability on multi-phase displacement behavior on time and saturation has yet to be considered.

CONCLUSIONS

- Predicted hysteresis between drainage and imbibition capillary pressure curves using the LOB network was much smaller than observed for experimental data.
- Increase in aspect ratio, adjustment of pore size distribution and correlation of neighboring pores by size gave a closer match to the magnitude of hysteresis but the amount of residual NWP was much higher than obtained by experiment.
- A close match with experimental values of residual NWP saturation was given by restricting snap-off to a minimum throat length based on the physics of interface stability of cylinders.
- After tuning to give an acceptable match with experimental primary drainage and the main imbibition curves, the model gave acceptable prediction of intermediate scanning curves obtained by experiment.
- The network model inventory provided data on the amount of continuous NWP versus disconnected NWP as a function of saturation for drainage and imbibition.
- Previously reported residual NWP blob size distributions obtained by 3D imaging were in close agreement with those computed for the tuned network.
- Comparison of experimental capillary pressure hysteresis data with predictions based micro CT imaging provide a stringent test of network modeling and the related issues of resolution and sample size.

ACKNOWLEDGEMENTS

Funding for this research was provided by BP, Chevron, Statoil and UW Enhanced Oil Recovery Institute.

REFERENCES

1. Prodanović, M., W.B. Lindquist, and R.S. Seright, "3D Image-Based Characterization of Fluid Displacement in a Berea Core", *Adv. Water Res*., (2007) **30**, 2, 214-226.
2. Fatt, I., "The Network Model of Porous Media. I. Capillary Pressure Characteristics", *Pet. Trans. AIME*, (1956) **207**, 144-159.
3. Chatzis, I., and F.A.L. Dullien, "Modeling Pore Structure by 2-D and 3-D Networks with Aplications to Sandstone", *J. Can.Petro. Tech*., (1977) **16**, 1, 97-108.
4. Wardlaw, N.C., Y. Li, and D. Forbes, "Pore-Throat Size Correlation from Capillary Pressure Curves", *Trans.Porous Media*, (1987) **2**, 6, 597-614.
5. Reeves, P.C., and M.A. Celia, "A Functional Relationship between Capillary Pressure, Saturation, and Interfacial Area as Revealed by a Pore-Scale Model", *Water Res. Research*, (1996) **32**, 8, 2345-2358.
6. Mason, G., and N.R. Morrow, "Capillary Behavior of a Perfectly Wetting Liquid in Irregular Triangular Tubes," *J. Colloid Interface Sci.,* (1991) **Jan**., 141, 262-74.

7. Bakke, S., and P.E. Øren, P.E., "3-D Pore-Scale Modeling of Sandstones and Flow Simulations in the Pore Networks", *Soc. Pet. Eng. J*., (1997) **2**, 136-149.
8. Øren, P.E., S. Bakke, and O.J. Arntzen, "Extending Predictive Capabilities to Network Models", *Soc. Pet. Eng. J*., (1998) *3*, 324-336.
9. Fenwick, D.H., and M.J. Blunt, "Three-dimensional Modeling of Three Phase Imbibition and Drainage", *Adv. Water Res.,* (1998) **21**, 2, 121-143.
10. Lerdahl, T.R., P.E. Øren, and S. Bakke, "A Predictive Network Model for Three-Phase Flow in Porous Media", presented at the SPE/DOE IOR, Tulsa, OK, (2000).
11. Man, H.N., and X.D. Jing, "Network Modelling of Wettability and Pore Geometry Effect on Electrical Resistivity and Capillary Pressure", *J. Pet. Sci. Engr*., (1999) **24**, 2-4, 255-267.
12. Patzek, T.W., "Verification of a Complete Pore Network Simulator of Drainage and Imbibition", *Soc. Pet. Eng. J*., (2001) **6**, 144-156.
13. Valvatne, P.H., and M.J. Blunt, "Predictive Pore-Scale Modeling of Two-Phase Flow in Mixed Wet Media", *Water Resour. Res*., (2004) **40**, 7, W07406.
14. Mason, G**.,** "A Model of the Pore Space in a Random Packing of Equal Spheres", *J. Colloid Interface Sci.*, (1971) **35**, 279-287.
15. Mason, G., "Determination of the Pore-Size Distributions and Pore-Space Interconnectivity of Vycor Porous Glass from Adsorption-Desorption Hysteresis Capillary Condensation Isotherms", *Proc. Royal Society, London A,* (1988) **415**, 453-486.
16. Bryant, S., D. Mellor, and C. Cade, "Physically Representative Network Models of Transport in Porous Media", *AIChE Journal*, (1993) **39**, 3, 387-396.
17. Knackstedt, M.A., A.P. Sheppard, and M. Sahimi, "Pore Network Modelling of Two Phase Flow in Porous Rock: The Effect of correlated Hetrogeneity", *Adv. Water Res*., (2001) **24**, 3-4, 257-277.
18. Sok, R.M., M.A. Knackstedt, A.P. Sheppard, W.V. Pinczewski, W.B. Lindquist, A. Venkatarangan, and L., Paterson, "Direct and Stochastic Generation of Network Models from Tomographic Images; Effect of Topology on Residual Saturation", *Transp. Porous Media*, (2002) **46**, 2-3, 345-372.
19. Øren, P.E., and S. Bakke, "Reconstruction of Berea Sandstone and Pore-Scale Modelling of Wettability Effects", *J. Pet. Sci. Eng*., (2003) **39**, 177-199.
20. Chatzis, I. and N.R. Morrow, "Correlation of Capillary Number Relationships for Sandstones," *Soc. Pet. Eng. J*., (1984), **24**, 5, 555-562.
21. Li, Y., and N.C. Wardlaw, "The Influence of Wettability and Critical Pore-Throat Size Ratio on Snap-off", *J. Colloid Interface Sci.*, (1986). **109**, 2, 461–472.
22. Raeesi, B., "Measurement and Pore-Scale Modelling of Capillary Pressure Hysteresis in Strongly Water-Wet Sandstones", Ph.D. diss., U. of Wyoming, Laramie, WY, (2012).
23. Gerhard, J.I., and B.H. Kueper, "Prediction of Interfacial Areas during Imbibition in Simple Porous Media", *Adv.Water Res.*, (2003) **39**, 8,
24. Pentland, C.H., Y. Tanino, S. Iglauer, and M.J. Blunt, "Capillary Trapping in Water-Wet Sandstones: Coreflooding Experiments and Pore-Network Modeling", SPE 133798 presented at the SPE ATCE, Florence, Italy, Sept. (2010).
25. Morrow, N.R.: "Capillary Pressure Correlations for Uniformly Wetted Porous Media," *J. Can. Pet. Tech.,* (1976) **15**, 49.

26. Plateau, J., “Statique Experimentale et Therique des Liquides Soumis aux Seules Forces Moleculaires”, Vol. II, Gauthier-Villars, Paris (1873).
27. Mason, G**.,** "An Experimental Determination of Stable Length of Cylindrical Liquid Bubbles”, *J. Colloid Interfacial Sci*., (1970) **32**, 1, 172-176.
28. Erle, J.A., D.C. Dyson, and N.R. Morrow, “Liquid Bridges between Cylinders, in a Torus, and between Spheres”, *AICHE Journal* (1971) **17**, 1, 115-121.
29. Morrow, N.R. and C.C. Harris, “Capillary Equilibrium in Porous Material,” *Soc. Pet. Eng. J*., (1965) **5**, 15-24.
30. Chatzis, I., M.S. Kuntamukkula, and N.R. Morrow, "Effects of Capillary Number on the Microstructure of Residual Oil in Strongly Water-Wet Sandstones," *SPE Reservoir Eng.*, (1988) **3**, 902-12.
31. Kumar, M., J.P. Middleton, A.P. Sheppard, T.J. Senden, and M.A. Knackstedt, “Quantifying Trapped Residual Oil in Reservoir Core Material at the Pore Scale; Exploring the Role of Displacement Rate, Saturation History and Wettability” IPTC 14001, presented at the Int. Petro. Tech. Conf., Doha, Qatar, Dec. 7-9 (2009).